Breakdown kinetics and plasma evolution induced by IR and UV laser radiation

Vladimir I. Mazhukin[(1)], Vadim V. Nossov[(1)], Igor Smurov I.[(2)]

[(1)] Institute of Mathematical Modelling Russian Academy of Science, 125047 Moscow, Miusskaya 4a Russia.
[(2)] Ecole Nationale d'Ingénieurs de Saint-Etienne, 58 rue Jean Parot, F-42023 Saint-Etienne Cedex 2, France.

ABSTRACT

The results of mathematical modeling are presented related to the two qualitatively different stages of evolution of the laser-induced plasma.
The optical breakdown stage, characterized by high nonequilibrium of the undergoing processes, is described by means of the detailed kinetic model, with account for the basic collision and radiation transitions. In particular, a number of photo processes are included which are known to be important in the UV spectral range: resonance and non-resonance laser-induced excitation, excitation by the continuous spectrum radiation, ionization and recombination in the field of laser and continuous radiation, spontaneous radiative decay. The numerical analysis have shown that in the UV spectral range: (i) the resonance/non-resonance photoexcitation, and photoionization from the ground and the first excited states are the major mechanisms of optical breakdown; (ii) the non-resonance photoexcitation significantly depends on the broadened lines profile, determined by simultaneous contribution of the several broadening mechanisms; (iii) the breakdown threshold intensities are 2-3 orders of magnitude lower than the ones predicted by the «classical» approach.
The stage of gas-dynamic expansion of laser plasma is analyzed for the set-up corresponding to the Laser Shock Processing (LSP) of materials in the water-confined regime. Mathematical description of the plasma is performed in the frame of transient 2D Radiative Gas Dynamics (RGD). The studies performed indicate that the plasma expansion mode strongly depends on the laser wavelength. For the IR laser radiation the plasma expands in the form of the ionization wave, which propagates at the velocity much higher than the one of the shock wave and absorbs major part of the laser radiation. For the UV laser radiation the expansion proceeds in the form of the light-detonation wave. In both cases the plasma becomes opaque: for the IR effect it occurs over very short time, 3 – 5 ns, while for the UV range the process takes much longer time. When the laser intensity is increased, the peak intensity and the FWHM of the transmitted pulse tend to reach a saturation level.

Keyword: mathematical modeling, laser plasma, optical breakdown, nonequilibrium kinetics, radiative gas dynamics, plasma transmission.

1. INTRODUCTION

Action of powerful flux of laser radiation on a target leads to its evaporation, optical breakdown and development of plasma in evaporated substance. Plasma initiation near the irradiated surface changes qualitatively mode of thermal and mechanical effect of the laser radiation. Development of high-power eximer laser and promising aspect of their engineering applications (first of all, PLD technologies) put forward high-priority task to analyze effect of UV laser radiation on materials to determine, in particular, threshold conditions of intensive evaporation and plasma formation, and regularities of gas dynamic expansion. Self-consistent model of the phenomena should simultaneously describe processes in condensed in gaseous medium. Due to great complexity of the problem, it is rational to analyze some of its counterparts separately.

Optical breakdown of evaporated substance is the first stage of plasma evolution. It presents nonequilibrium transition of a medium from a state of slightly ionized gas transparent for the laser radiation to an opaque plasma state. Mechanisms of optical breakdown are not yet sufficiently studied and there are a number of subjects that require further analysis, for example, the frequency dependence of optical breakdown. It is known from experiments [1-3], that the threshold intensity G^* strongly depends on radiation frequency ω_l. The classical theory [4] predicts square dependence of the quantities $G^* \sim \omega_l^2$. However, experimental studies revealed significant deviation of observed threshold values from theoretical predictions

Laser-Assisted Microtechnology 2000, Vadim P. Veiko, Editor,
Proceedings of SPIE Vol. 4157 (2001) © 2001 SPIE · 0277-786X/01/$15.00

in visible and UV frequency ranges. The classical relation $G^* = \omega_l^2$ is fulfilled in the range of $\omega_l < 4.5 \cdot 10^{14}$ s^{-1} and its boundary corresponds approximately to the ruby laser frequency, $\hbar\omega$ = 1.79 eV. To analyze contribution of different breakdown mechanisms, it is necessary to consider population kinetics of multi-energy-level system. Corresponding mathematical model is presented in section 2 of the paper and is based on a large system of rate equations. The model accounts for a great number of collision and radiation transitions, and utilizes two-temperature approximation for description of energy balance. The model is applied to study the breakdown of Al vapor in a wide spectral range of laser action.

After completion of the optical breakdown stage the medium is in highly-ionized plasma state with temperature of several electron volts. Further gas dynamic expansion of the plasma proceeds under near-equilibrium conditions and is characterized by increasing contribution of plasma thermal radiation to the energy balance. This stage of the plasma can be described by the model of Radiative Gas Dynamics (RGD), which incorporates the system of gas dynamic equations and the radiation transfer equation. This approach is applied in Section 3 of the paper to analyze evolution of breakdown plasma in air under conditions typical for Laser Shock Processing (LSP) for laser action of the IR and UV range. The basis of LSP is utilization of high–power pressure pulse, generated by vapor plasma during the short pulse laser irradiation of metal target at the intensity >10^9GW/cm^2 [5-7]. Complex study of LSP of aluminum plate subjected to Nd-YAG laser pulses with duration of a 25 - 30 ns at a wavelength 1.06 μm was presented in Refs. [8, 9]. It was shown that if the LSP is executed in water confined regime, it allows to increase more than twice the amplitude and duration of the pressure pulse. Limiting factor of the approach is formation of secondary plasma at air - water interface, Fig. 6. The plasma partially or completely absorbs the incident laser radiation and as the result the pulse that actually effects on the target becomes shorter and weaker than the incident one. The main purpose of the study is to establish regularities of expansion, absorption and transmission of the air plasma.

2. KINETICS OF LASER-INDUCED BREAKDOWN OF ALUMINUM VAPOUR

Consider effect of laser beam with intensity G on a thin layer of evaporated matter with temperature T_0 and density ρ_0. Initially the vapor is in equilibrium state. At laser intensity is lower than a threshold value G^*, the vapor remains transparent and laser radiation goes through the layer without absorption. At $G > G^*$, initial absorption rate appears to be sufficient to induce avalanche-like ionization of the vapor. Threshold intensity and breakdown period depend on properties of evaporated material: temperature, density, configuration of electron shells and ionization potentials, as well as on laser action parameters: intensity, duration and radiation frequency. In the IR range, main mechanism of laser energy dissipation is the inverse Bremsstrahlung phenomenon. In the UV range, a number of photo-processes are known to play an important role.

2.1. ATOM TRANSITIONS

Mathematical model for analysis of level-by-level kinetics strongly depends on electron configuration [10,11]. The present model for neutral atom of Al accounts for the following collisional and photo-induced transitions:

Type of transition	*Participating particles*	*Notation of rate coefficient*
Electron impact ionization	$Al_m + e \rightarrow Al_i + e + e$	α_m [cm^3 s^{-1}]
Three-particle recombination	$Al_i + e + e \rightarrow Al_m + e$	β_m [cm^6 s^{-1}]
Collisional excitation/ de-excitation	$Al_m + e \leftrightarrow Al_n + e,\ n > m$	k_{mn}, r_{mn} [cm^3 s^{-1}]
Spontaneous radiative decay	$Al_n \rightarrow Al_m + \hbar\omega_{mn},\ n > m$	A_{mn} [s^{-1}]
Laser-induced photoionization	$Al_m + \hbar\omega_l \rightarrow Al_i$	ν^l_m [s^{-1}]
Laser-induced photorecombination	$Al_i + e + \hbar\omega_l \rightarrow Al_m + \hbar\omega_l$	R^l_m [cm^3 s^{-1}]
Laser-induced photoexcitation	$Al_m + \hbar\omega_l \rightarrow Al_n,\ n > m$	ν^l_{mn} [s^{-1}]
Continuum radiation photoionization	$Al_m + \hbar\omega_c \rightarrow Al_i$	ν^c_m [s^{-1}]
Continuum radiation photorecombination	$Al_i + e + \hbar\omega_c \rightarrow Al_m + \hbar\omega_c$	R^c_m [cm^3 s^{-1}]
Continuum radiation photoexcitation	$Al_m + \hbar\omega_c \rightarrow Al_n,\ n > m$	ν^c_{mn} [s^{-1}]

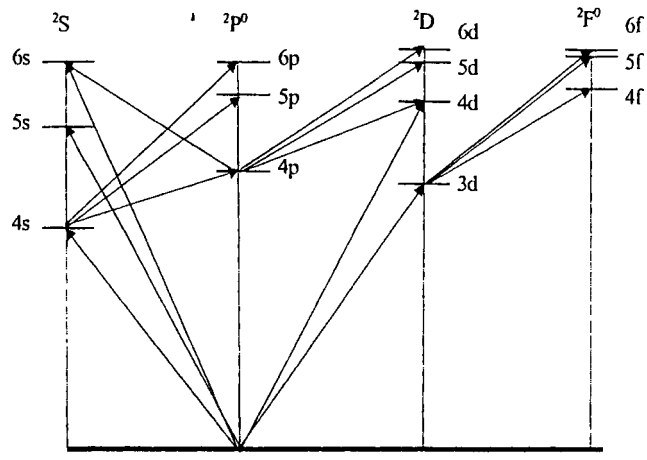

Figure 1. Collisional transitions in Al atom

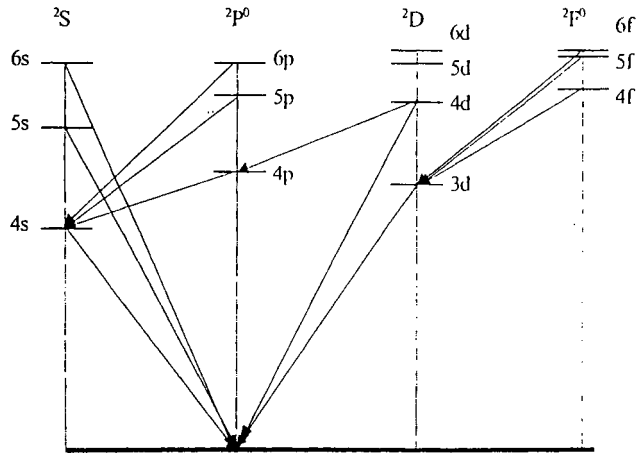

Figure 2. Radiative transitions in Al atom

Here Al_m, m =0, ..., M denote atoms of Al in the ground (m = 0) and excited states; Al_i stands for single charged ion, e is electron, $\hbar\omega_l$, $\hbar\omega_c$ are photons of laser and continuous spectrum radiation. The collisional and spontaneous radiative transitions included of the model are presented in Figs. 1,2.

2.2. SYSTEM OF EQUATIONS

Concentrations of neutral N_0, excited N_m, charged N_i particles and electrons N_e, $N_i \approx N_i$ are described by nonlinear system of rate equations:

$$\frac{dN_0}{dt} = -\sum_{j=1}^{M}(k_{0j}N_0 - r_{j0}N_j)N_e - (\alpha_0 N_0 - \beta_0 N_i N_e)N_e + \sum_{j=1}^{M} A_{j0}N_j(x) - \\ - \sum_{j=1}^{M}\nu_{0j}^{c}\left(N_0 - \frac{g_0}{g_j}N_j\right) - \nu_{01}^{\ell}\left(N_0 - \frac{g_0}{g_1}N_1\right) - \left(\nu_0^{l} + \nu_0^{c}\right)N_0 + \left(R_0^{c} + R_0^{\ell}\right)N_i N_e \tag{1}$$

$$\frac{dN_m}{dt} = \sum_{j=0}^{m-1}(k_{jm}N_j - r_{mj}N_m)N_e - \sum_{j=m+1}^{M}(k_{mj}N_m - r_{jm}N_j)N_e - (\alpha_m N_m - \beta_m N_i N_e)N_e + \\ + \nu_{m-1,m}^{\ell}\left(N_{m-1} - \frac{g_{m-1}}{g_m}N_m\right) + \sum_{j<m}^{M}\nu_{jm}^{c}\left(N_j - \frac{g_j}{g_m}N_m\right) - \sum_{j>m}^{M}\nu_{mj}^{c}\left(N_m - \frac{g_m}{g_j}N_j\right) \\ - \sum_{j=0}^{m-1}A_{mj}N_m + \sum_{j=m+1}^{M}A_{mj}N_j + \left(R_m^{c} + R_m^{\ell}\right)N_i N_e - \left(\nu_m^{c} + \nu_m^{\ell}\right)N_m, \qquad m = 1,\ldots,M \tag{2}$$

$$\frac{dN_i}{dt} = \frac{dN_e}{dt} = \sum_{m=0}^{M}(\alpha_m N_m - \beta_m N_i N_e)N_e + \sum_{m=1}^{M}\left(\nu_m^{c} + \nu_m^{\ell}\right)N_m - \sum_{m=1}^{M}\left(R_m^{c} + R_m^{\ell}\right)N_i N_e \tag{3}$$

where g_j denote statistical weights of the excited states. Energy balance of the nonequilibrium plasma is characterized by two temperatures: T_e for the electrons and T_g for the heavy particles (atoms and ions). The equations are written as:

$$\frac{3d(N_e T_e)}{2dt} = \left((\mu G - \frac{3}{2}\delta(T_e - T_g))(\nu_{en} + \nu_{ei}) - \sum_{m=0}^{M}Q_{m,J} - \sum_{m=0}^{M-1}Q_{m,\Delta E}\right)N_e + Q_\Phi; \tag{4}$$

$$\frac{3}{2}\frac{d}{dt}(N_g T_g) = \frac{3}{2}\delta(T_e - T_g)(\nu_{en} + \nu_{ei})N_e; \tag{5}$$

$$\mu = \frac{4\pi e^2}{mc\left(\omega^2 + (\nu_{en} + \nu_{ei})^2\right)}, \quad \delta = \frac{2m}{M}, \quad N_g = \sum_{m=0}^{M} N_m$$

$$Q_{m,\Delta E} = \sum_{j=m+1}^{M} \Delta E_{jm}(k_{mj}N_m - r_{jm}N_j), \quad Q_{m,J} = J_m(\alpha_m N_m - \beta_m N_i N_e),$$

$$Q_{\Phi} = \sum_{m=0}^{M}\left[\left(\hbar\omega_\ell - J_m\right)\left(\nu_m^\ell N_m + R_m^\ell N_e N_i\right) + \left(\hbar\omega_c - J_m\right)\left(\nu_m^c N_m + R_m^c N_e N_i\right)\right].$$

Here m, M are masses of electrons and atoms, ν_{en}, ν_{ei} are the frequencies of electron - neutral and electron - ion collisions, E_m denotes the excitation energy of the m-th state, J_0, J_m are ionization energy of ground and excited states. The system is completed by initial conditions

$$t = 0: \qquad N_0 = N_0^0; \quad N_m = N_m^0, m = 1,\ldots,M; \quad N_i = N_e = N_e^0; \quad T_e = T_g = T_o; \tag{6}$$

where N_0^0, N_m^0, N_e^0, are equilibrium values determined by Saha-Boltzmann distribution at the temperature T_0 and density ρ_0. The differential model (1)-(6) allows to analyze transient non-equilibrium processes in spatially homogeneous plasma.

2.3. RESULTS AND DISCUSSION

The mathematical model is applied to study the optical breakdown of Al vapor induced by laser action of the wide spectral range: from CO_2 laser frequency $\omega_l = 2.83\cdot10^{13}$ s^{-1} ($\hbar\omega_l = 0.117$ eV, $\lambda_l = 10.6$ μm) to $\omega_l = 1.55\cdot10^{15}$ s^{-1} ($\hbar\omega_l = 6.42$ eV, $\lambda_l = 0.193$ μm), which is 1.8 times higher than the ArF laser frequency. The objective is to determine dependence of threshold intensity G^* on the laser wavelength λ_l, $G^* = G^*(\lambda_l)$. Following approach of Refs. [10,12] we postulate that optical breakdown have occurred in the medium if the $\nu_{en} < \nu_{ei}$ condition is fulfilled. The threshold intensity G^* is further defined as minimal laser intensity that initiates optical breakdown.

influence of duration and temporal intensity distribution of the laser pulse on the optical breakdown can be rather important and necessarily should be taken into account while comparing numerical predictions and experimental results. However, typical rates of the elementary processes included into the model are rather different and their particular contribution to the optical breakdown can manifest itself at different time instants. Therefore the analysis is performed for constant intensity (top - hat) laser pulse and the pulse duration is not restricted in advance.

The initial state of the metal vapor is defined by setting its temperature T_0 and density ρ_0 approximately equal to the temperature and density at outer boundary of Knudsen layer, adjacent to the target surface with temperature equal to the equilibrium boiling temperature, $T_b = 2720$ K = 0.234eV. Thus, $T_0 = 0.2$eV, $N_0^0 = M \cdot \rho_0 = 6\cdot10^{18}$ cm^{-3}, $N_e^0 = 3\cdot10^{14}$ cm^{-3}.

Two spectral dependencies of the threshold intensity $G^*(\lambda_l)$ are shown in Figure 3. The curve 1 corresponds to the theoretical dependency [4], and is computed by model, which accounts only for collisional transitions and spontaneous radiative decay. The curve 2 is predicted using the complete model (1)-(6). The two dependencies coincide in the IR range $\hbar\omega_l \in 0.117 \div 1.17$ eV. For example, predicted threshold value for CO_2 and Nd-YAG lasers are $G^* = 6\cdot10^5$ W/cm^2 and $G^* = 6\cdot10^7$W/cm^2 respectively. For remainder part of spectral range, the curve 2 locates below the curve 1 and is characterized by several sharp drops at frequencies, corresponding to selective excitations of electronic transitions. Deviation of two curves indicates qualitative difference of the optical breakdown mechanisms in IR and visible/UV range. As it will be shown, the difference is explained by non-monotone increase of photo-process contribution with decreasing wavelength. Numerical analysis of specific contribution for each type of the photo-processes was performed and it was determined that the two of them: the laser-induced photoionization and photoexitation play a major role.

Photoionization. Relative contribution of the process is illustrated in Figure 4: the curve 1 and 2 are the same as in Figure 3 and the curve 3 presents the $G^*(\lambda_l)$ dependence determined by the classical model, which additionally includes the laser photoionization and neglects all the rest photo-induced reactions. The " non-classical " dependence, curve "3", is non-monotone and locates below the classical one. The non-monotone behavior of the curve is explained by following factors: the threshold nature of the process as the $\hbar\omega_l > J_m$ should satisfied for the m-th level ionization, strong dependence

of photoionization cross-section on the frequency $\sigma_m \sim \omega_l^{-3}$ and the main quantum number, $\sigma_m \sim m^{-5}$. Two minimum on the curve "3" correspond to ionization energies of the ground $3p$ (J_0 = 5.98 eV) and the first excited $4s$ (J_1= 2.84 eV) levels. Exclusion of photo-excitation from the model leads to disappearance of sharp drops, initially observed at the frequencies corresponding to the resonance excitation of the energy levels, curves "2" and "3". Thus, in UV range the laser-induced photoionization is an important process that decreases the threshold intensity by the 1-2 orders of magnitude.

Resonance photoexcitation. The laser-induced resonance photoexcitation is realized if the laser frequency is equal to the frequency of transition between two bond electronic states, $\omega_l = \omega_{mn}$. The contribution of this process is shown in Fig.5 – again, the curve "1" is the classical dependence, while the model used to compute the curve "2a" additionally accounts for laser–induced photoionization and resonance photoexitation. The resonance photoexitation manifests in appearance of sharp and deep vertical drops on the $G^*(\lambda_l)$ curve. The process is the most pronounced for the first four excited states. For example, the resonance excitation of the 1st level reduces the threshold intensity to $G^* \approx 10^2$ W/cm^2, and its contribution is one order of magnitude higher then the one of the ground level photoexcitation. Contribution of the resonance photoexcitation of the 2nd and the 3rd level are comparable to the ground level photoionization. The great contribution of the process is explained by its high cross-section $\sigma_m \sim 10^{-12}$ cm^2 which is 5 - 6 orders of magnitude higher than the one of photoionization. Thus, the resonance photoexitation selectively affects the breakdown and can reduce the threshold intensity by the 4 - 6 orders of magnitude.

Non-resonance laser photoexcitation. If there is no precise resonance between a bond-bond electronic transition and the laser radiation $\omega_l \neq \omega_{mn}$, the laser radiation can be effectively absorbed in the "wings" of the spectral broadening function $S_{mn}(\omega)$. This phenomenon lies in basis of the non-resonance photoexitation. The $G^*(\lambda_l)$ dependence determined with account for the photoionization and both the resonance and non-resonance photoexitation is presented by the curve "2" in Fig.4. In the IR range, the non-resonance process reduces the threshold intensity by 2-10 times. In the UV range, the influence is much stronger and can reduce the threshold by several orders of magnitude.

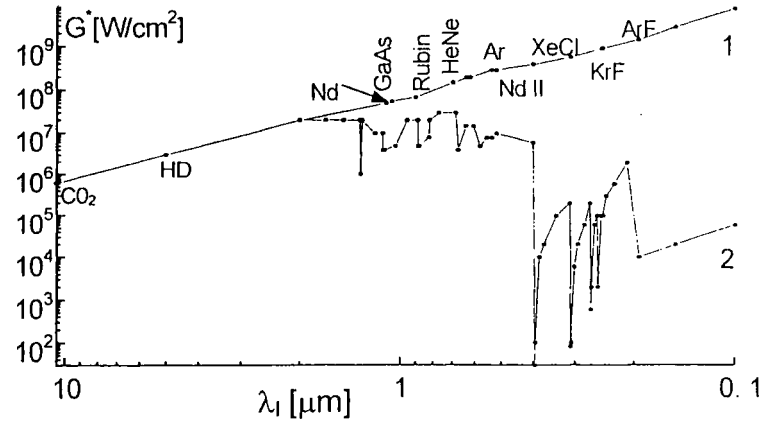

Figure 3. Spectral dependence of the breakdown threshold intensity. 1: the model includes the collisional processes and spontaneous decay (the classical model); 2: the complete model (1)-(6).

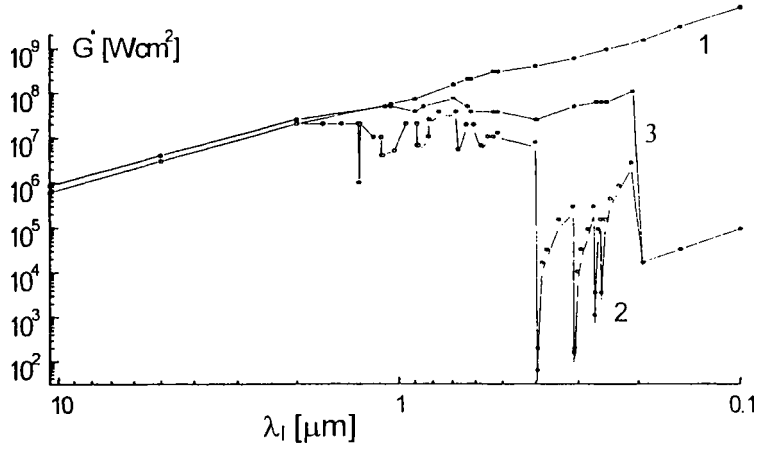

Figure 4. Spectral dependence of the breakdown threshold intensity. 1: the classical model; 2: the complete model (1)-(6); 3: the classical model + laser-induced photoionisation.

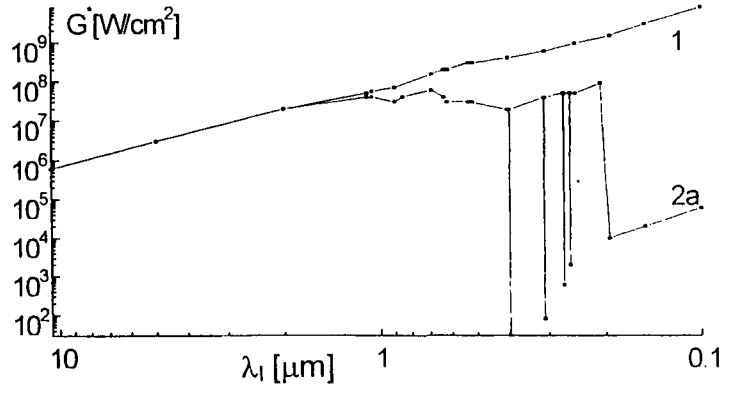

Figure 5. Spectral dependence of the breakdown threshold intensity. 1: the classical model; 2a: the classical model + laser-induced photoionisation + resonance photoexitation

3. MODELING OF BREAKDOWN PLASMA IN AIR DURING LASER SHOCK PROCESSING

Typical scheme of LSP in water-confined regime is presented in Fig. 6. Metal target is covered by water layer, laser radiation propagates perpendicular to the target surface and leads to plasma formation at metal-water and water-air interface. Self-adjusted description of the processes in both media in 2D case presents very complex computational problem. However, absorption and transmission of air plasma can be predicted by using more simple model, if it is assumed that thin plasma layer already exists at the interface at the beginning of laser action.

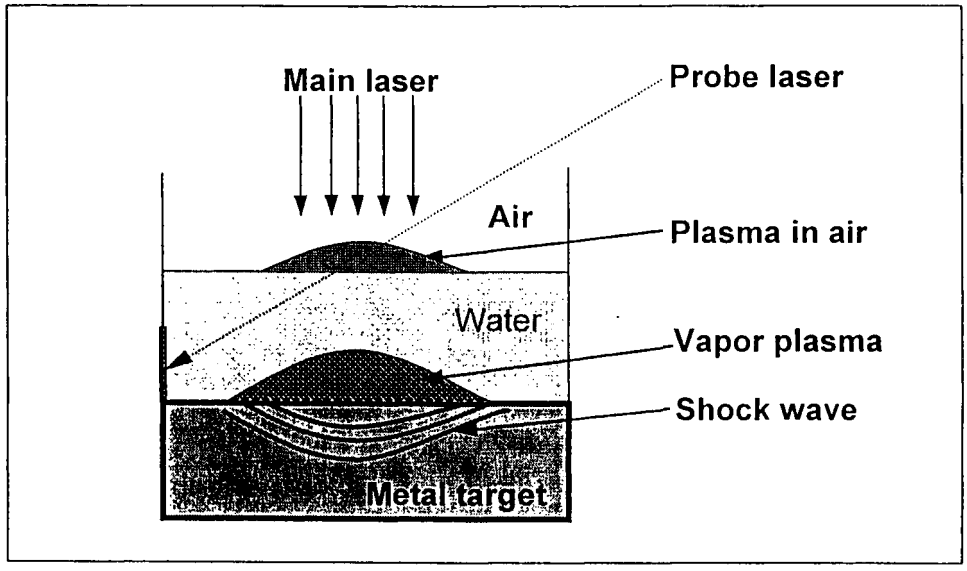

Figure 6: Scheme of Laser Shock Processing in the water-confined regime accompanied by breakdown plasma formation in air

3.1. PHYSICO-MATHEMATICAL MODEL

The problem has axial symmetry and is solved in cylindrical coordinate system introduced in air domain. Z-axis coincides with the laser beam axis and follows outward drawn normal to water surface, r-axis is directed along the air-water interface. Description of the plasma evolution is performed by the complete system of radiative gas dynamics (RGD), supplemented by the transfer equation for the laser radiation and the two equations of the state [14]:

$$\frac{\partial \rho}{\partial t}+\frac{1}{r}\frac{\partial}{\partial r}(r\rho u)+\frac{\partial}{\partial z}(\rho v)=0; \tag{7}$$

$$\frac{\partial(\rho u)}{\partial t}+\frac{1}{r}\frac{\partial}{\partial r}\left(r\rho u^2\right)+\frac{\partial}{\partial z}(\rho u v)=-\frac{\partial(p+\omega)}{\partial r}; \tag{8}$$

$$\frac{\partial(\rho v)}{\partial t}+\frac{1}{r}\frac{\partial}{\partial r}(r\rho u v)+\frac{\partial}{\partial z}\left(\rho v^2\right)=-\frac{\partial(p+\omega)}{\partial z}; \tag{9}$$

$$\frac{\partial(\rho\varepsilon)}{\partial t}+\frac{1}{r}\frac{\partial}{\partial r}(r\rho u\varepsilon)+\frac{\partial}{\partial z}(\rho v\varepsilon)=-p\left[\frac{1}{r}\frac{\partial(ru)}{\partial r}+\frac{\partial v}{\partial z}\right]-\left[\frac{1}{r}\frac{\partial W_r}{\partial r}+\frac{\partial W_z}{\partial z}\right]+\left[\frac{\partial G}{\partial z}\right]; \tag{10}$$

$$\vec{\Omega}\,grad\,I_\nu+\kappa_\nu I_\nu=\kappa_\nu I_{\nu,eq}; \qquad \vec{W}=\int_0^\infty\partial\nu\int_{-1}^{1}\mu\partial\mu; \tag{11}$$

$$\frac{\partial G}{\partial z}-\kappa G=0; \tag{12}$$

$$p=p(\rho,T), \quad \varepsilon=\varepsilon(\rho,T). \tag{13}$$

Here t, r, z are the time and spatial coordinates; ρ stands for the density; u, v are the components of velocity vector; p, ω denote the pressure and artificial viscosity; ε represents the volumetric density of internal energy; W_r, W_z are the components of total radiation flux of the plasma $\vec{W}$; G denotes the laser radiation intensity; $\vec{\Omega}$ is the unit vector of direction of a photon; I_ν, $I_{\nu,eq}$ are the spectral intensity and spectral equilibrium intensity of radiation; κ_ν denotes the spectral absorption coefficient.

The equation system is supplemented by the initial and boundary conditions:

$t = t_0$

$$u = v = 0, \qquad 0 \le (r \times z) \le (L_r \times L_z)$$
$$T = T_{hot},\ \rho = \rho_{hot}, \quad 0 \le (r \times z) \le (l_r \times l_z) \tag{14}$$
$$T = T_0,\ \rho = \rho_0, \qquad (l_r \times l_z) < (r \times z) \le (L_r \times L_z)$$

$r = 0$: $$u = 0, \quad \partial\rho/\partial r = \partial v/\partial r = \partial P/\partial r = 0, \quad W_r = 0; \tag{15}$$

$z = 0$: $$v = 0, \quad \partial\rho/\partial z = \partial u/\partial z = \partial P/\partial z = 0, \quad cU = \sigma T^4; \tag{16}$$

$r = L_r$: $$p = p_0, \quad \rho = \rho_0, \quad u = v = 0, \quad W_r = -cU/2; \tag{17}$$

$z = L_z$: $$p = p_0, \quad \rho = \rho_0, \quad u = v = 0, \quad W_z = -cU/2, \tag{18}$$
$$G = G_0 \exp\left(-(t/\tau)^2\right)\exp\left(-(r/R)^2\right).$$

Absorption coefficient of laser radiation κ is specified by the following formula:

$$\kappa = \frac{8\pi e^6}{mhc3(6\pi mk)^{1/2}} \frac{N_e \sum_{z=1}^{Z_{max}} z^2 N_z}{\nu^3 T^{1/2}} \left(1 - exp\left(-\frac{h\nu}{T}\right)\right) \tag{19}$$

where N_e, N_z are concentration of electrons and ions with charge z (the $z = 0$ index corresponds to neutral atom); Z_{max} denotes maximum charge of ions accounted in the model; h, m, e are the Plank constant, mass and charge of electrons. Charge composition of the plasma in equilibrium approximation is described by Saha equations.

3.2. RESULTS OF MODELLING

Computations are performed under the following conditions: the domain $0 \le (r \times z) \le (L_r \times L_z)$ is considered to be filled by undisturbed cold air at temperature $T(0, r, z) = T_0$ and $\rho\ (0, r, z) = \rho_0$. The $z = 0$ plane correspond to the free surface of the confined water. Initial stage of laser effect that involves evaporation, optical breakdown of the evaporated matter and plasma initiation, is modeled by specifying the initial hot domain $0 \le (r \times z) \le (l_r \times l_z)$ at temperature $T(0, r, z) = T_{hot}$ and $\rho(0, r, z) = \rho_0$. The gas-plasma region is irradiated by laser pulses of $2\tau = 34$ ns duration and peak intensity $G_0 = 6$-13 GW/cm^2 at either $\lambda = 1.06$ μm or $\lambda = 0.353$ μm. The presented results correspond to $L_r = L_z = 2$ cm, $r_{hot} = 2R = 0.3$ cm, $\rho_0 = 1.25 \times 10^{-3}$ cm^{-3}, $T_0 = 0.03$ eV, $\rho_{hot} = \rho_0$; $T_{hot} = 1.05$ eV, $z_{hot} = 50$ μm for IR effect and $T_{hot} = 2$ eV, $z_{hot} = 100$ μm for UV effect.

Results for IR and UV laser radiation at $G_0 = 10$ GW/cm^2 are presented in Figures 7-10. Distributions of temperature, density and electron concentration are shown at two instants of time, $t \approx 0$ ns and $t \approx 34$ ns, which correspond to peak intensity and termination of the laser pulse. The results for the IR effect are shown in Figs. 7, 9, and the ones for the UV effect are presented in Figs. 8, 10. For the IR laser radiation the energy is absorbed in thin plasma layer due to the high absorption coefficient, that results in plasma expansion in the form of ionization wave. The ionization front propagates at the velocity approximately 5 times higher than the one of the shock wave, Fig. 11. Presence of preferential direction for propagation of the ionization wave results in strongly asymmetric shape of the plasma pattern that is stretched along the z-axis, Fig.9. For the UV laser radiation the absorption rate is much lower, the energy release proceeds volumetrically that leads to realization of another mechanism of the plasma propagation referred to as light-detonation regime, Fig. 12. The expansion at all the directions proceeds at approximately the same speed, and the shape of the plasma pattern is close to the spherical one, Fig. 10.

Different expansion mechanisms result in different transmission of the plasma for the IR and UV radiation, 1.06 μm and 0.353 μm. Presented in Figs. 13, 14 are the transmission coefficients determined as $G(r = 0, z = 0) / G(r = 0, z = L_z)$ that characterize fraction of laser radiation transmitted through the plasma. The numerically predicted transmission coincides well with the experimental data [8].

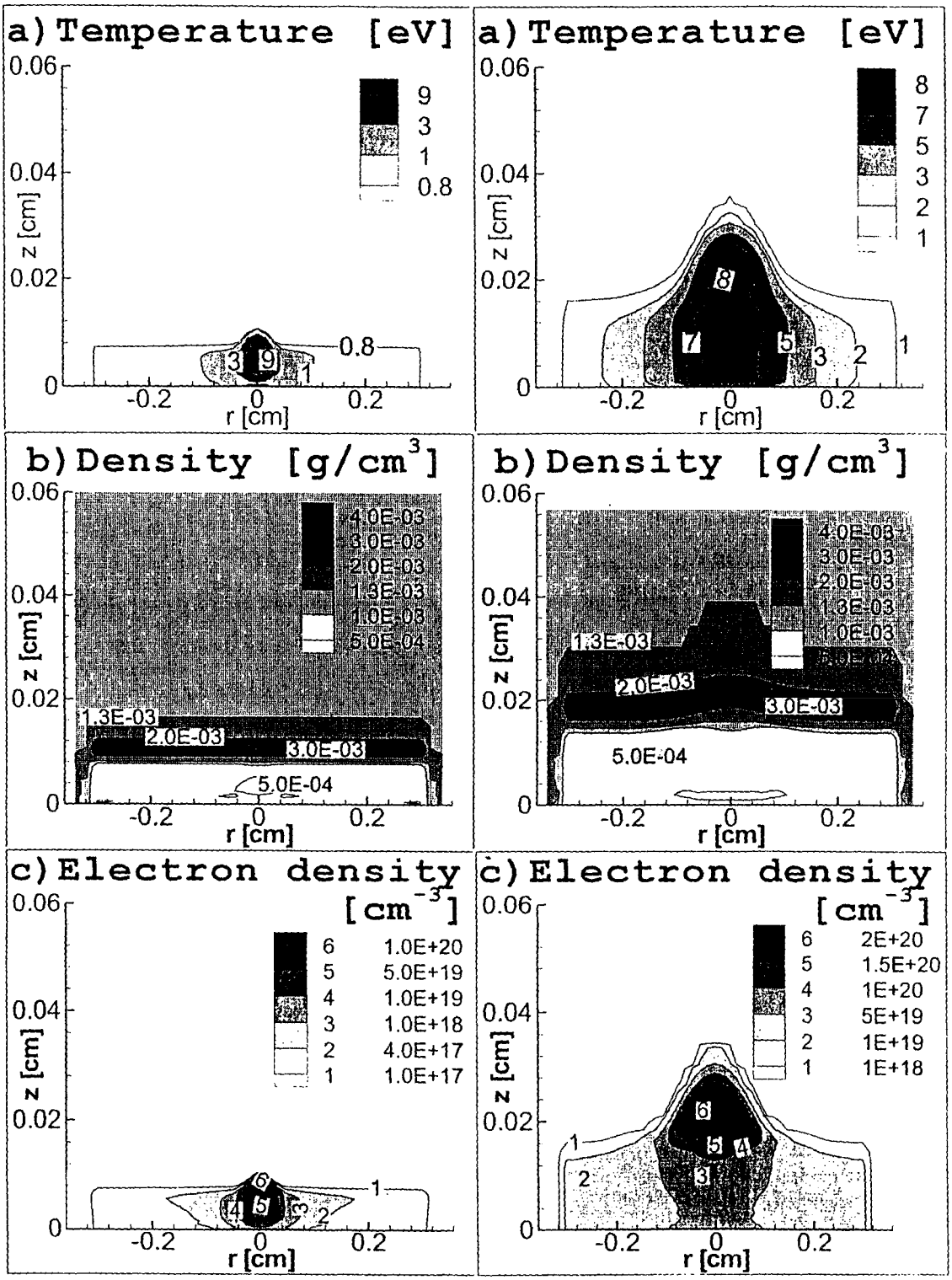

Figure 7: Contour plots of the computational domain subjected to laser pulse at $\lambda = 1.06\mu m$, at $t = 0$ ns (peak of the pulse): (a) temperature, (b) density, (c) electron concentration.

Figure 8: Contour plots of the computational domain subjected to laser pulse at $\lambda = 0.353\mu m$ at $t = 0$ ns (peak of the pulse): (a) temperature, (b) density, (c) electron concentration.

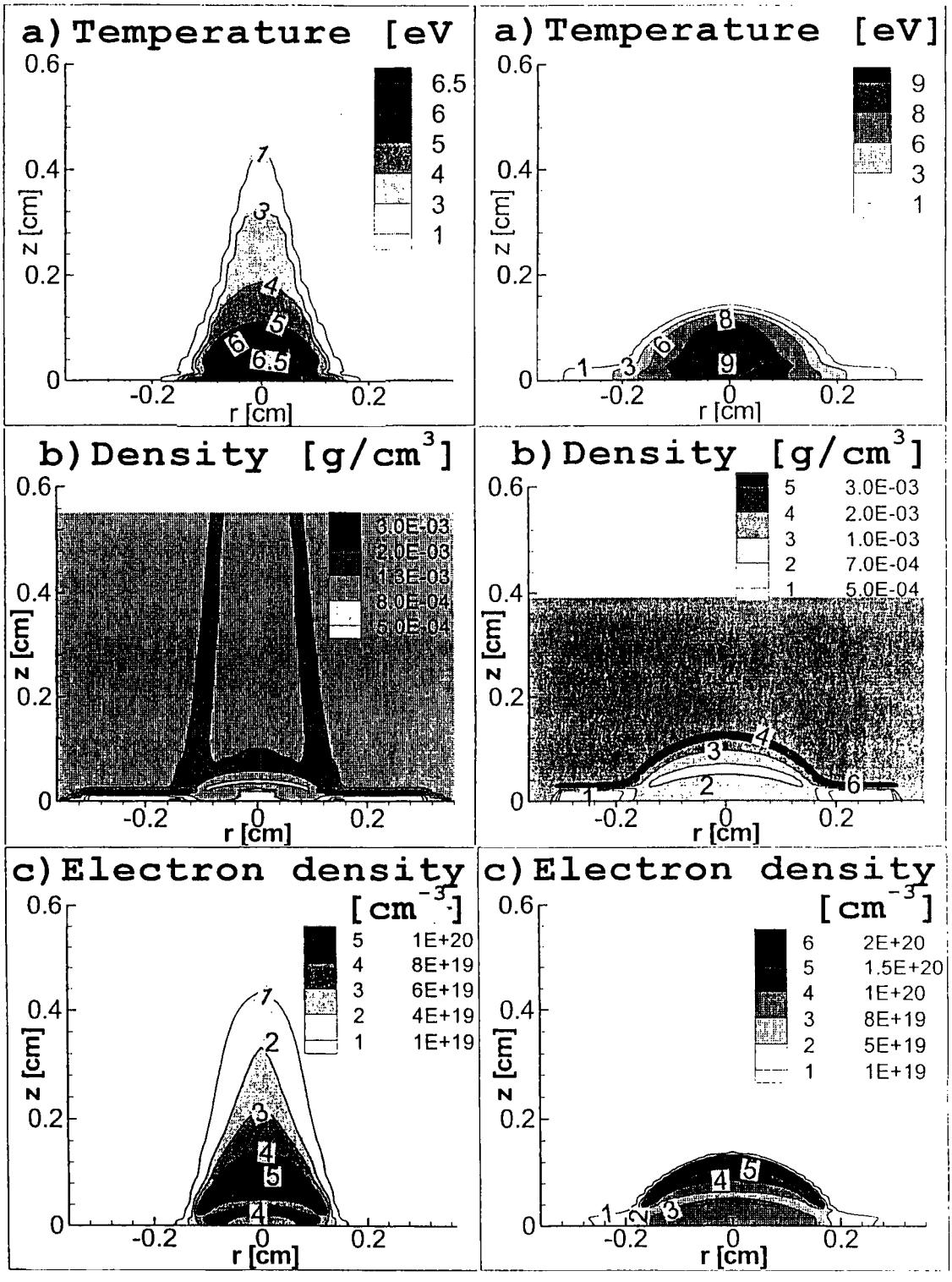

Figure 9: Contour plots of the computational domain subjected to laser pulse at $\lambda = 1.06\mu m$, at t = 35 ns (completion of the pulse): (a) temperature, (b) density, (c) electron concentration.

Figure 10: Contour plots of the computational domain subjected to laser pulse at $\lambda = 0.353\mu m$, at t = 35 ns (completion of the pulse): (a) temperature, (b) density, (c) electron concentration.

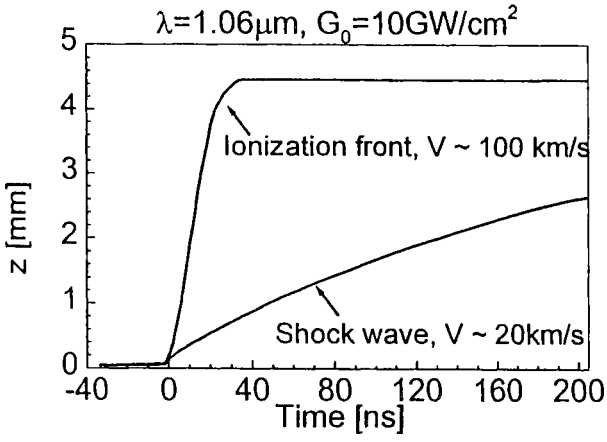

Figure 11: Coordinates of the shock wave and ionization front, $\lambda = 1.06$ μm.

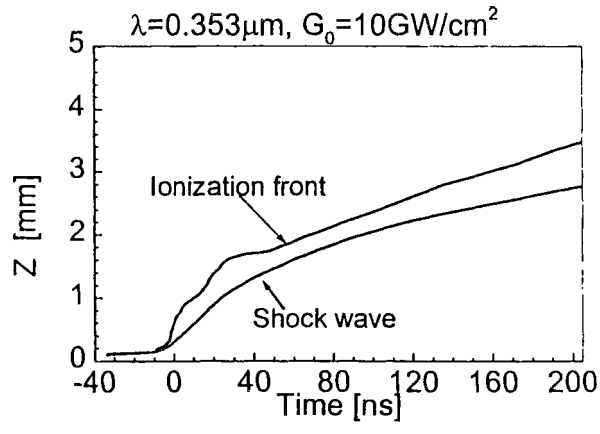

Figure 12: Coordinates of the shock wave and ionization front, $\lambda = 0.353$ μm.

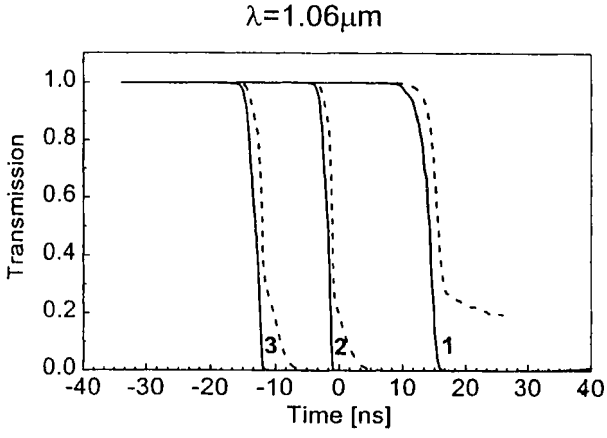

Figure 13: Transmission coefficient of plasma at $\lambda = 1.06$ μm (solid lines), and $\lambda = 0.514$μm (dashed lines) for laser radiation at $\lambda = 1.06$μm of intensity $G_0 = 6$ GW/cm^2 - (1); $G_0 = 10$ GW/cm^2 - (2); $G_0 = 13$ GW/cm^2 - (3).

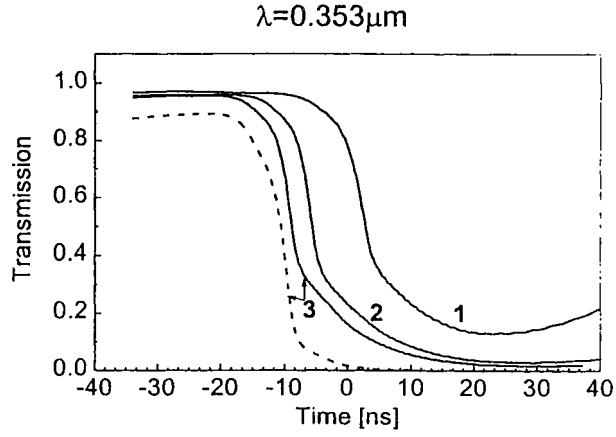

Figure 14: Transmission coefficient of plasma at $\lambda = 0.353$ μm (solid lines), and $\lambda = 0.514$μm (dashed lines) for laser radiation at $\lambda = 0.353$μm of intensity $G_0 = 6$ GW/cm^2 - (1); $G_0 = 10$ GW/cm^2 - (2); $G_0 = 13$ GW/cm^2 - (3).

4. CONCLUSION

The modeling is performed for the two qualitatively different stages of evolution of the laser-induced plasma: the stage of optical breakdown and the gas-dynamic plasma evolution. The results indicate the strong dependence of the phenomena on the laser wavelength.

The advanced kinetic model is developed and applied to study the breakdown of Al vapor induced by laser radiation of the IR, visible and the UV ranges. Numerical analysis shows that in UV-range:

- Resonance/ non-resonance excitation and ionization from the ground and first excited states are the major mechanisms of optical breakdown.
- Non-resonance photo-excitation depends significantly on the broadened line profile, formed by simultaneous

contribution of several broadening mechanisms.

- The threshold radiation intensities in the UV-range are 2-3 orders of magnitude lower, then the ones predicted by classical approach.

In earlier studies the role of photoionisation has been pointed out [2,13]), but the contribution of photoexcitation was not studied earlier.

Modeling of the air plasma is performed, induced by IR λ = 1.06 μm and UV λ = 0.355 μm laser radiation in the intensity range of G_0 = 6 -13 GW/cm^2. The results indicate strong non-linear coupling between thermal, radiation and gas-dynamics processes in the plasma. Interaction of the processes, ultimately, determines plasma transmission, which is the basic parameter for optimization of irradiation regime. The main physical results are:

- The expansion of the plasma has qualitative differences for the IR and UV laser radiation and proceeds in the ionization and light-detonation regimes, respectively.
- The typical plasma temperature and maximum electron concentration predicted are ~10eV and $\approx 5 \cdot 10^{20}$ cm^{-3}, the critical electron concentration for the considered radiation wavelengths is not reached.
- Thermal radiation of plasma contributes significantly to redistribution of energy inside the plasma domain and, for the UV effect, forms the domain of pre-ionization ahead of the shock wave.
- For the UV laser wavelength the screening effect of plasma manifests itself at lower intensity, but the time needed for plasma to become completely opaque is 20 – 30 ns, while for the IR action the process takes only 3 – 5 ns.

5. ACKNOWLEDGEMENTS

The work was partially supported by the European Commission under the Copernicus CP96-0080 Project (VITEWE).

6. REFERENCES

1. J. A.Woodroffe, J. Hsia, and A. Ballatyne, *Appl. Phys. Lett.*, v. 36, p.14, 1980.
2. D. I. Rosen, J. Mittledorf, G. Kothandaraman et al., *J. Appl. Phys.*, v. 53, p. 3190, 1982.
3. V. P. Ageev, A. A.Gorbunov, V. P. Danilov et al., *J.Quantum Electronics*, v.10 p. 2451, 1983.
4. Ya. B. Zeldovich, and Yu. P. Raizer, *Physics of Shock waves and High Temperature Hydrodynamics Phenomena I* (Academic, New York, 1967).
5. P. Fairand, and B. A. Wilcox, *J. Appl. Phys.*, v. 43, p. 3893, 1972.
6. H. Clauer, B. P. Fairand, and J. Holbrook, In: *Shock Waves and High Strain Phenomena in Metals – concepts and applications,* edited by L. Murr (Plenum, New York, 1981), p. 675.
7. P. Peyre, R. Fabbro, L. Berthe, and C. Dubouchet, *J. Laser Appl.*, v. 8, p. 135, 1996.
8. L. Berthe, R. Fabbro, P. Peyre, and E. Bartnicki, *Europ. Phys. J. Appl. Phys.*, v. 3, p. 215, 1998.
9. L. Berthe, R. Fabbro, P. Peyre, and E. Bartnicki, *J. Appl. Phys.*, p. 85, p. 7552, 1999.
10. V. I. Mazhukin, I. Gusev, I. Smurov, and G. Flamant, *Microchemical J.*, v. 50, p. 413, 1994.
11. V. I. Mazhukin, I. Gusev, I. Smurov, and G. Flamant, *J.de Physique IV*, v. 4, C4-101, 1994.
12. M. Mitchner, and C. H. Kruger. Partially Ionized Gases. (Wiley,New York, 1973).
13. A. M. Popov. *J. Engineering Physics*, v. 52, p. 2105, 1982.
14. V. I. Mazhukin, I. Smurov, and G. Flamant, *J. Comp. Phys.*, v. 112, p. 78, 1994.